

# High Order Finite Elements for Lagrangian Computational Fluid Dynamics

Truman E. Ellis

Advisor: Dr. Faisal Kolkailah

LLNL Mentors: Dr. Robert Rieben and Dr. Tzanio Kolev

Department of Aerospace Engineering  
California Polytechnic State University  
San Luis Obispo, CA

[ellis.truman@gmail.com](mailto:ellis.truman@gmail.com)

April 23, 2010

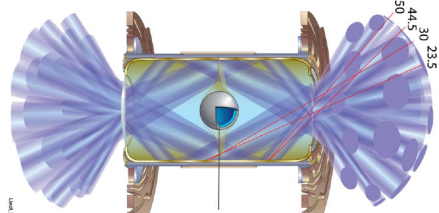
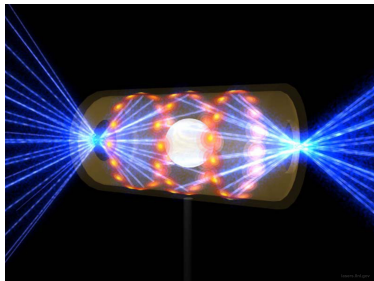


This work performed under the auspices  
of the U.S. Department of Energy by  
Lawrence Livermore National Laboratory  
under Contract DE-AC52-07NA27344  
LLNL-PRES-416883, -416822



# Outline

- Introduction
  - Frameworks
  - Overview
- Theory
  - Euler Equations
  - Lagrangian Mesh Motion
  - Finite Element Method
  - Semi-Discrete Formulation
  - Methods Considered
  - Bi-Quadratic Methods
- Numerical Results
  - Static Momentum Solve
  - Sod Shock Tube
  - Acoustic Wave
  - Noh Implosion
  - Saltzman Piston
  - Sedov Explosion
  - Computational Efficiency
- Conclusions

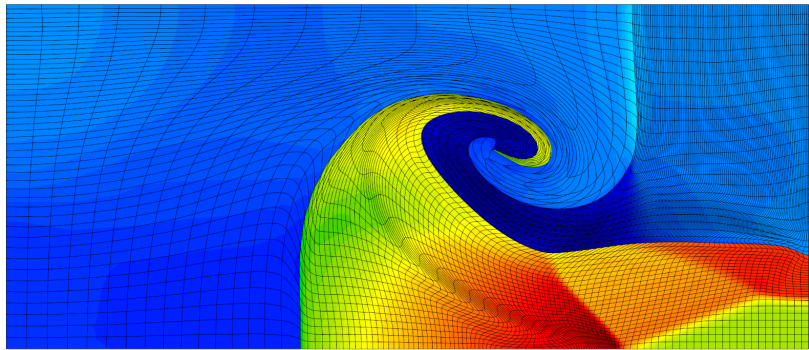


courtesy llnl.gov

# Frameworks

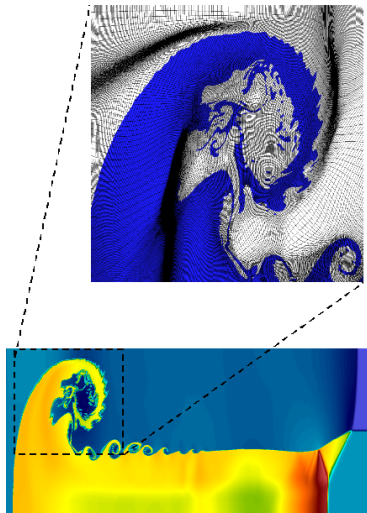
## Typical simulation frameworks

- Eulerian: Traditional CFD - material is fluxed through a stationary mesh
- Lagrangian: Mesh nodes follow material particles - mesh moves with the material
- Arbitrary Lagrangian-Eulerian (ALE): Lagrangian until mesh tangling is detected.  
Fluid simulation is paused as the mesh is relaxed.  
Stationary state variables are advected through the moving mesh.



Lagrangian simulation of a triple point shock

- This thesis develops advanced finite element discretization methods for Lagrangian hydrodynamics.
- The goal is to improve the current staggered grid hydro (SGH) algorithms in multi-material ALE codes with respect to:
  - symmetry preservation
  - energy conservation
  - artificial viscosity discretization
  - hourglass-mode instabilities
- We consider a general framework for solving the Euler equations with the following features:
  - allows for high order field representations
  - allows for curved element geometry
  - exact energy conservation by construction
  - reduces to classical SGH under simplifying assumptions



# Glossary

We consider several different hydro methods which make use of various finite element spaces. The specific finite element spaces considered in this talk are:

- Q0: discontinuous constant finite element space on quadrilaterals
- Q1: continuous bi-linear finite element space on quadrilaterals
- Q2: continuous bi-quadratic finite element space on quadrilaterals
- Q1d: discontinuous bi-linear finite element space on quadrilaterals
- Q2d: discontinuous bi-quadratic finite element space on quadrilaterals

Each hydro method is designated by a pair of finite element spaces:

- A continuous kinematic space
- A discontinuous thermodynamic space

For example:

Q2-Q1d uses continuous quadratic velocities and positions with discontinuous bi-linear pressures and densities. All methods are assumed to have a discontinuous constant energy space.

# Euler Equations in a Lagrangian Frame

The Euler equations of gas dynamics in a Lagrangian reference frame can be written in differential form as:

Momentum Conservation:  $\rho \frac{dv}{dt} = -\vec{\nabla} p + \dots$

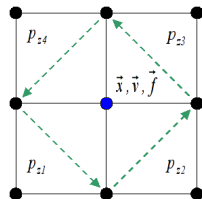
Mass Conservation:  $\frac{1}{\rho} \frac{d\rho}{dt} = -\vec{\nabla} \cdot \vec{v}$

Energy Conservation:  $\rho \frac{de}{dt} = -p \vec{\nabla} \cdot \vec{v} + \dots$

Equation of State:  $p = EOS(e, \rho)$

Typically, these equations are solved on a staggered spatial grid [1,2] where thermodynamic variables are approximated as piece-wise constants defined on zone centers and kinematic variables are defined on the nodes.

Spatial gradients are computed using finite volume and/or finite difference methods:



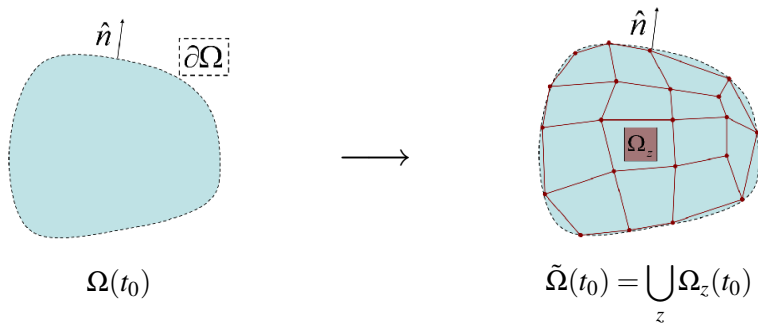
[1] R. Tipton, CALE Lagrange Step, unpublished LLNL report, 1990

[2] M. Wilkins, Calculations of Elastic-Plastic Flow, In Methods of Computational Physics, 1964

# Domain Decomposition

We propose a general semi-discrete FEM approach to solving the Euler equations in a Lagrangian frame. A semi-discrete method is only concerned with the spatial approximation of the continuum equations.

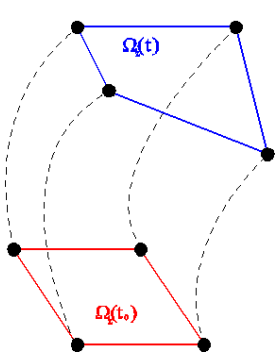
To begin, we decompose the continuum domain at an initial time into a set of non-overlapping discrete volumes (zones). The union of these volumes forms the computational mesh:



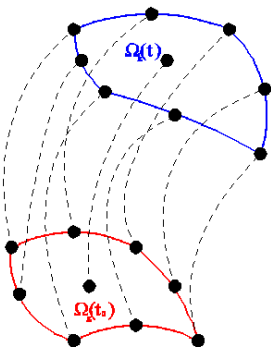
The motion of the continuous medium will therefore be described by the motion of only a finite number of particles (mesh vertices, edge midpoints, etc )

# Lagrangian Mesh Motion

After deformation in time, zones are reconstructed based on particle locations, thus defining the moved mesh.

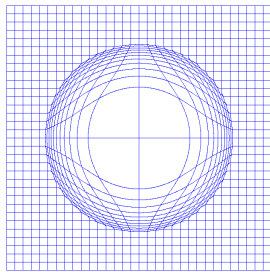


Q1 (Bi-Linear) Approximation



Q2 (Bi-Quadratic) Approximation

This reconstruction process has an inherent geometric error.



Initial Cartesian mesh deformed with the exact solution of the Sedov blast wave problem.

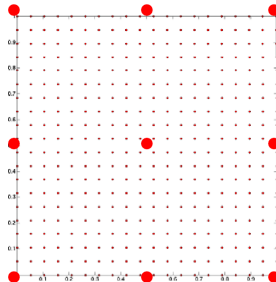
This built in geometric error motivates the use of (higher order) finite elements which can use the additional particle degrees of freedom to more accurately represent continuous deformations.

# Lagrangian Mesh Motion: Animation

# Curved Geometries

Finite element basis functions are defined on a reference (unit) zone. To compute quantities on an arbitrary mesh zone, we use the Jacobian matrix which defines the geometric transformation (or mapping) from reference space:

Reference Space:

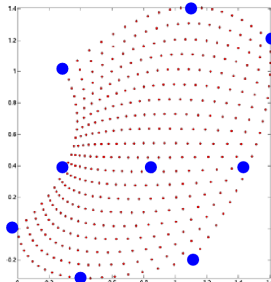


$$\Phi : \hat{\vec{x}} \rightarrow \vec{x}$$
$$(\mathbf{J}_z)_{i,j} = \frac{\partial x_j}{\partial \hat{x}_i}$$

$$\phi(\hat{\vec{x}})$$

$$\vec{\nabla} \phi(\hat{\vec{x}})$$

Physical Space:



$$\phi(\vec{x}) = \hat{\phi}(\Phi^{-1}(\vec{x}))$$

$$\vec{\nabla} \phi = J_Z^{-1} \vec{\nabla} \hat{\phi}$$

A standard Q1 mapping gives zones with straight edges, while Q2 mappings produce curved zones. Note that we can have Q1 elements defined with a Q2 mapping and vice versa. The finite element reference degrees of freedom are in general different from the nodes of the mapping.

# Basis Functions

We approximate each of the continuum fields with a basis function expansion, where the expansion coefficients are independent of space:

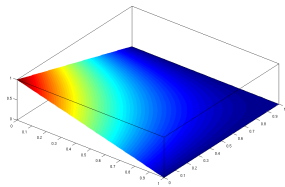
$$\text{Velocity: } \vec{v}(\vec{x}, t) \approx \sum_i^{N_v} \mathbf{v}_i(t) w_i(\vec{x})$$

$$\text{Internal Energy: } e(\vec{x}, t) \approx \sum_i^{N_e} \mathbf{e}_i(t) \theta_i(\vec{x})$$

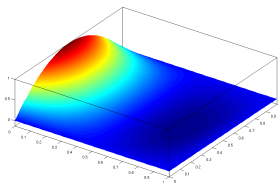
$$\text{Pressure: } p(\vec{x}, t) \approx \sum_i^{N_p} \mathbf{p}_i(t) \phi_i(\vec{x})$$

$$\text{Density: } \rho(\vec{x}, t) \approx \sum_i^{N_p} \rho_i(t) \psi_i(\vec{x})$$

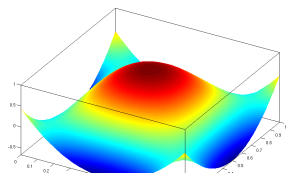
Our formulation is general; we are free to choose various types of basis functions. However, stability requires that certain choices are not independent<sup>[1]</sup> (e.g. pressure and velocity.)



Q1 (Bi-Linear) basis function  
4 DOF per Quad



Q2 (Bi-Quadratic) basis function  
9 DOF per Quad



Q2 basis function with degrees of freedom at the 9 Gauss-Legendre quadrature points

[1] See for example: D. Arnold et. al., Differential Complexes and stability of Finite Element Methods, 2005.

# Semi-Discrete Momentum Conservation

To derive a semi-discrete momentum conservation law, we begin with a variational formulation:

$$\rho \frac{d\vec{v}}{dt} = -\vec{\nabla} p \implies \int_{\tilde{\Omega}(t)} \left( \rho \frac{d\vec{v}}{dt} \right) \cdot \vec{w}' = \int_{\tilde{\Omega}(t)} (\vec{\nabla} p) \cdot \vec{w}' = \int_{\tilde{\Omega}(t)} p (\vec{\nabla} \cdot \vec{w}') - \int_{\partial \tilde{\Omega}(t)} p (\vec{w}' \cdot \hat{n})$$

Multiply by vector valued test function, integrate over computational mesh

Perform integration by parts

Inserting our basis function expansions and applying Galerkin's method by picking the velocity basis as the test function yields the following linear system of equations:

$$\int_{\tilde{\Omega}(t)} \left( \rho \sum_i \frac{dv_i}{dt} \vec{w}_i \right) \cdot \vec{w}_j = \int_{\tilde{\Omega}(t)} \sum_i p_i \phi_i (\vec{\nabla} \cdot \vec{w}_j)$$

Write in matrix / vector form



$$\mathbf{M} \frac{d\mathbf{v}}{dt} = \mathbf{D}^T \mathbf{p}$$

The **Mass** and **Derivative** matrices are computed zone by zone and assembled to form global systems:

$$(\mathbf{M}_z)_{ij} = \int_{\tilde{\Omega}(t)} \rho (\vec{w}_i \cdot \vec{w}_j)$$

The symmetric positive definite mass matrix describes how matter is distributed in space

$$(\mathbf{D}_z)_{ij} = \int_{\tilde{\Omega}(t)} \phi_i (\vec{\nabla} \cdot \vec{w}_j)$$

The rectangular derivative matrix maps between pressure and velocity spaces. This matrix is a discrete version of the Div operator. Its adjoint (transpose) is the Grad operator

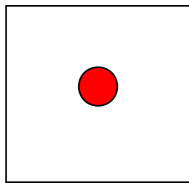
# Computing Mass and Derivative Matrices

In practice, we compute the mass and derivative matrices by integrating over the reference volume using a change of variables:

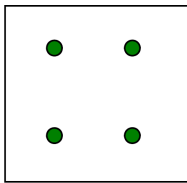
$$\int_{\Omega(t)} f = \int_{\tilde{\Omega}(t)} (f \circ \Phi) |\mathbf{J}_z|$$

The integrals are computed using Gaussian quadrature of a specified order. For certain integrands and quadrature rules, this can be computed exactly:

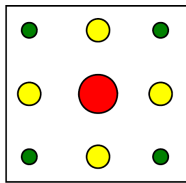
$$\int_{\tilde{\Omega}(t)} (f \circ \Phi) |\mathbf{J}_z| \approx \sum_{n=1}^{N_q} \alpha_n \{f \circ \Phi) |\mathbf{J}_z|\}_{\hat{x}=\hat{q}_n}$$



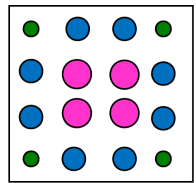
2D Order 1 Gauss-Legendre rule (exact for Q1)



2D Order 2 Gauss-Legendre rule (exact for Q3)



2D Order 3 Gauss-Legendre rule (exact for Q5)



2D Order 4 Gauss-Legendre rule (exact for Q7)

## Semi-Discrete Mass Conservation

We define the zonal mass moments in a natural manner:  $\mathbf{m}_{z,i} = \int_{\Omega_z(t)} \rho \psi_i$

The Lagrangian description requires that:  $\frac{d\mathbf{m}_{z,i}}{dt} = 0$

From the representation:  $\rho(\vec{x}, t) \approx \sum_i \rho_i(t) \psi_i(\vec{x})$  it follows that:  $\mathbf{m}_{z,i} = \sum_j \rho_{z,j} \int_{\Omega_z(t)} \psi_i \psi_j$

In matrix form we have:  $\mathbf{m}_z = \mathbf{M}_z^\rho \rho_z$  where  $(\mathbf{M}_z^\rho)_{i,j} = \int_{\Omega_z(t)} \psi_i \psi_j$

If we impose the stronger condition:  $\frac{d}{dt} \int_{\Omega(t)} \rho \psi = 0$  for any function  $\psi$

then we obtain the *strong mass conservation principle*:

$$\rho(t) |\mathbf{J}(t)| = \rho(t_0) |\mathbf{J}(t_0)|$$

Note that, in general, the density defined by the above equation is *not polynomial*.

Note that both generalizations imply the standard zonal mass conservation

# Energy Conservation, EOS, and Artificial Viscosity

We treat the energy conservation equation in a local manner. Consider the special case of piece-wise constant internal energies; we have the following semi-discrete energy conservation law:

$$\mathbf{m}_z \frac{d\mathbf{e}_z}{dt} = -\mathbf{p}_z \mathbf{D}_z \mathbf{v}_z = -(\mathbf{p}_z \mathbf{D}_z) \mathbf{v}_z = -\sum_i \vec{f}_i \cdot \vec{v}_i$$

The equation of state is evaluated point-wise according to

$$p = EOS(\rho, e)$$

Artificial viscosity is added to the corner forces to counteract shock compression

$$\vec{f}_Q = \vec{\nabla} \cdot (\mu \vec{\nabla} \vec{v})$$

Variational Formulation  
⇒

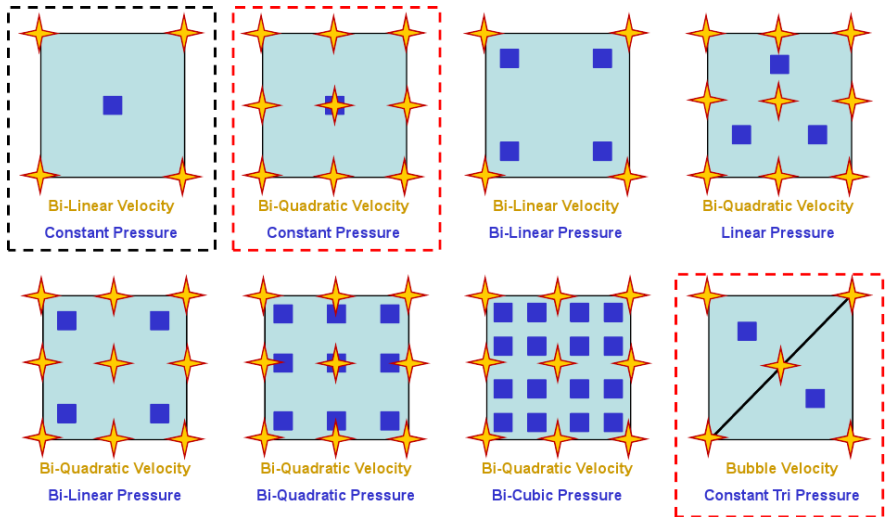
$$\vec{f}_Q = - \int_{\Omega} \mu \vec{\nabla} \vec{v}_z \cdot \vec{\nabla} \phi = -\mathbf{S}_z \mathbf{v}_z$$

where

$$(\mathbf{S}_z)_{i,j} = \int_{\bar{\Omega}} \rho_z \mu_z \left( \mathbf{J}_z^{-1} \vec{\nabla} \phi_i \right) \cdot \left( \mathbf{J}_z^{-1} \vec{\nabla} \phi_j \right) |\mathbf{J}_z|$$

The viscosity coefficient has adjustable linear term to control oscillations and quadratic term to handle shock smoothing. Artificial viscosity is usually turned off in expansion.

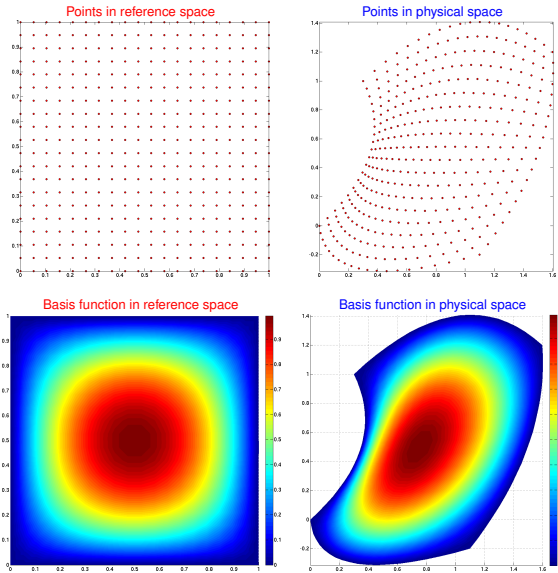
# Mixed Finite Elements



# High Order Methods Using the Q2 Basis

For each Q2 zone, we track 9 independent vertices (coordinates, velocities, accelerations etc ) which define the quadratic mapping from reference space to physical space. This mapping is defined using the Q2 Jacobian matrix, which is a function:

$$\begin{aligned} J(x,y) = & [(y - 1)(2y - 1)(4x - 3)x_1 \\ & + (y - 1)(2y - 1)(4x - 1)x_2 \\ & + y(2y - 1)(4x - 1)x_3 \\ & + y(2y - 1)(4x - 3)x_4 \\ & - 4(y - 1)(2y - 1)(2x - 1)x_5 \\ & - 4y(y - 1)(4x - 1)x_6 \\ & - 4y(2y - 1)(2x - 1)x_7 \\ & - 4y(y - 1)(4x - 3)x_8 \\ & + 16y(y - 1)(2x - 1)x_9, \\ & (4y - 3)(x - 1)(2x - 1)x_1 \\ & + x(4y - 3)(2x - 1)x_2 \\ & + x(4y - 1)(2x - 1)x_3 \\ & + (4y - 1)(x - 1)(2x - 1)x_4 \\ & - 4x(4y - 3)(x - 1)x_5 \\ & - 4x(2y - 1)(2x - 1)x_6 \\ & - 4x(4y - 1)(x - 1)x_7 \\ & - 4(2y - 1)(x - 1)(2x - 1)x_8 \\ & + 16x(2y - 1)(x - 1)x_9 ] \end{aligned}$$



# High Order Methods Using the Q2 Basis

For each zone in the computational mesh, we compute the following matrices using Gauss-Legendre quadrature of a specified order.:

The symmetric positive definite 9 by 9 mass matrix describes how matter is distributed within the Q2 zone

$$(\mathbf{M}_z)_{i,j} \equiv \int_{\hat{\Omega}_z} \rho_z(w_i w_j) |\mathbf{J}_z|$$

The **rectangular** derivative matrix maps between the pressure and velocity spaces. This matrix is a discrete version of the **Div** operator. Its adjoint (transpose) is the **Grad** operator

$$(\mathbf{D}_z^x)_{i,j} \equiv \int_{\hat{\Omega}_z} \phi_i(\mathbf{J}_z^{-1} \vec{\nabla} w_j) \cdot \{1, 0\} |\mathbf{J}_z|$$
$$(\mathbf{D}_z^y)_{i,j} \equiv \int_{\hat{\Omega}_z} \phi_i(\mathbf{J}_z^{-1} \vec{\nabla} w_j) \cdot \{0, 1\} |\mathbf{J}_z|$$

The symmetric positive definite 9 by 9 stiffness matrix is a discrete version of the second order DivGrad operator. It is used to compute the artificial viscosity

$$(\mathbf{S}_z)_{i,j} \equiv \int_{\hat{\Omega}_z} \mu_z(\mathbf{J}_z^{-1} \vec{\nabla} w_i)(\mathbf{J}_z^{-1} \vec{\nabla} w_j) |\mathbf{J}_z|$$

The bulk of the computational effort is in computing the high order Jacobian matrix. However, this can be computed once per quadrature point and shared between each matrix.

For the remaining examples, we apply **mass lumping** to the mass matrix to eliminate the need for a global linear solve. In addition, we compute the mass matrix only once as an initial condition.

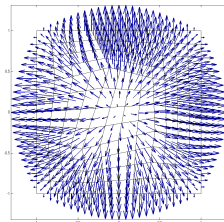
# Static Momentum Equation Solve Convergence Study

In this simple test, we project an analytic pressure function onto a randomly perturbed mesh and solve for the resulting accelerations:

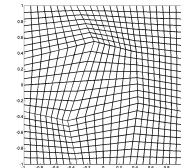
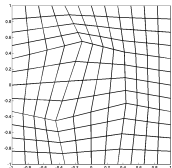
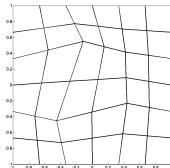
$$p(x, y) = \cos\left(\frac{\pi}{2}x\right)\cos\left(\frac{\pi}{2}y\right)$$

$$ma = -\nabla p$$

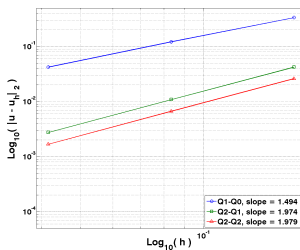
$$\mathbf{M}\mathbf{a} = -\mathbf{D}^T \mathbf{p}$$



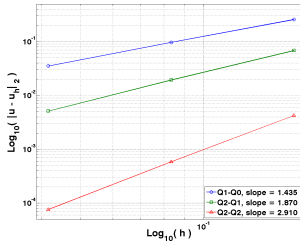
Randomly perturbed base line mesh and a sequence of refinements



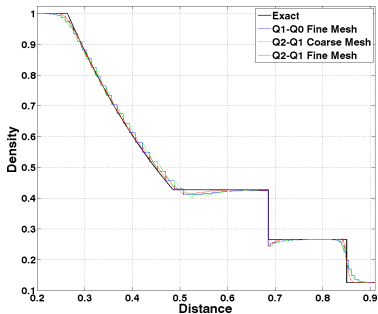
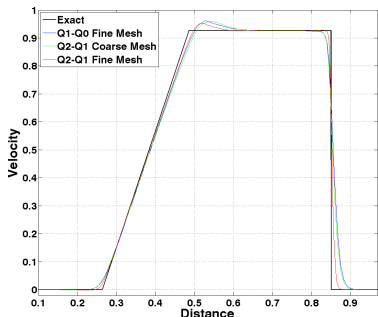
Lumped mass matrix



Full linear solve

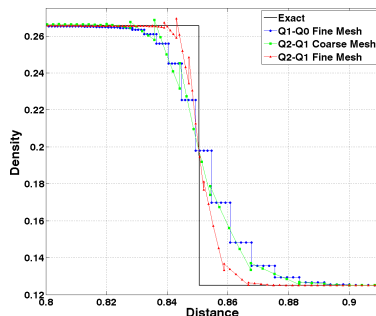
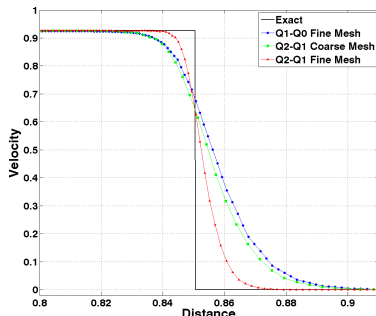


# 1D Sod Shock Tube: Velocity and Density



- We consider two meshes: A coarse 60 zone mesh and fine 120 zone mesh
- For each method,  $q_{lin} = q_{quad} = 1.0$ , no monotonic limiter is used
- We acknowledge this is sub-standard for Q1 (i.e. limiters make a difference); however, this a fair comparison between each method
- For each zone, 5 plot points are evaluated
- Each method captures contact discontinuity exactly due to discontinuous thermodynamic basis

# 1D Sod Shock Tube: Velocity and Density (Zoomed View)



- We consider two meshes: A coarse 60 zone mesh and fine 120 zone mesh
- For each method,  $q_{lin} = q_{quad} = 1.0$ , no monotonic limiter is used
- We acknowledge this is sub-standard for Q1 (i.e. limiters make a difference); however, this a fair comparison between each method
- For each zone, 5 plot points are evaluated
- Each method captures contact discontinuity exactly due to discontinuous thermodynamic basis

# The Acoustic Wave Problem

## Tests:

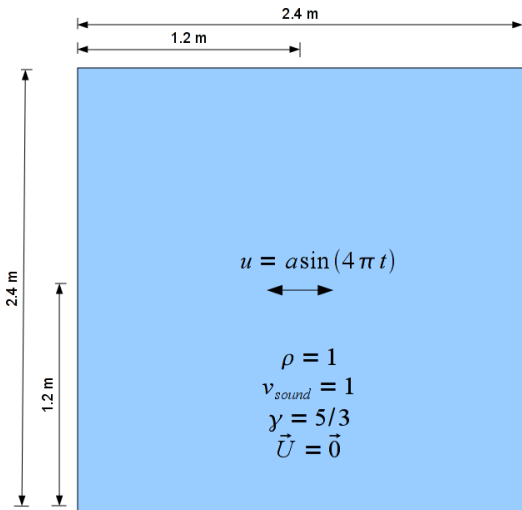
- Methods independent of artificial viscosity
- Spurious velocity and pressure modes
- Correct wave speed

## Ideally:

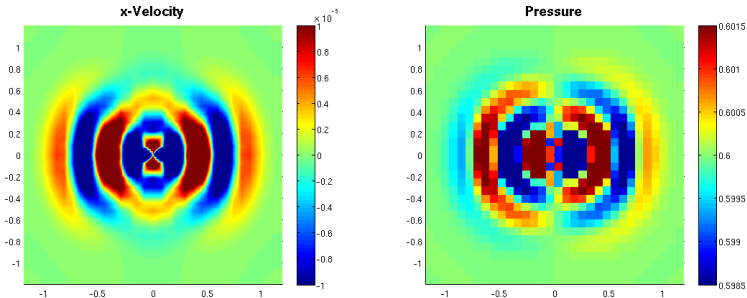
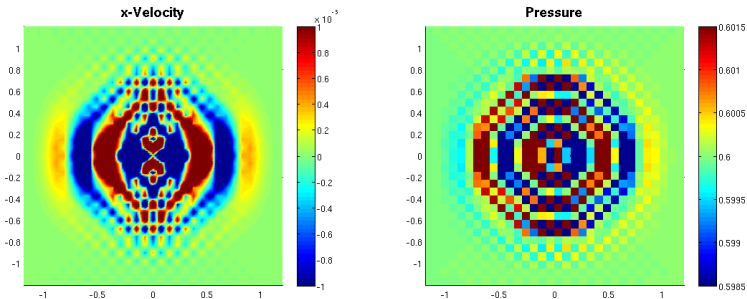
- Smooth waves
- No spurious modes
- Wave speed = 1

## Known Issues:

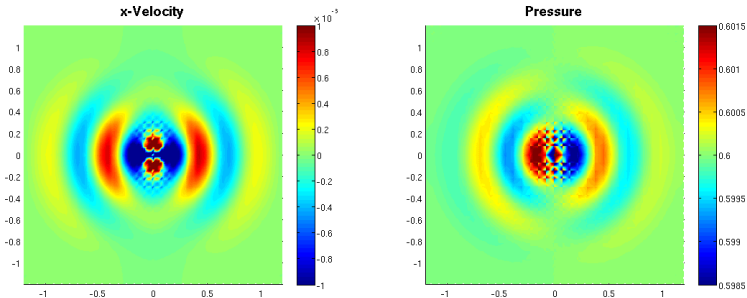
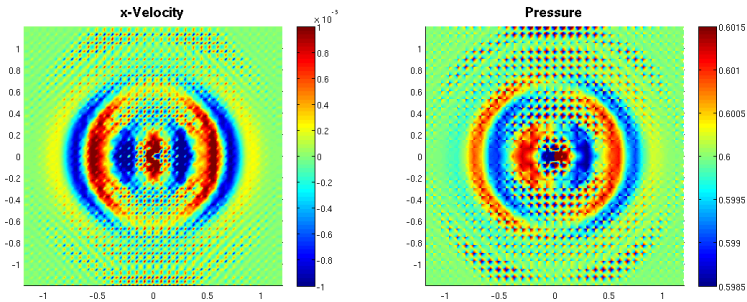
- No analytical solution
- Does not converge under refinement



# Acoustic Wave Problem: Q1-Q0



# Acoustic Wave Problem: Q2-Q1d



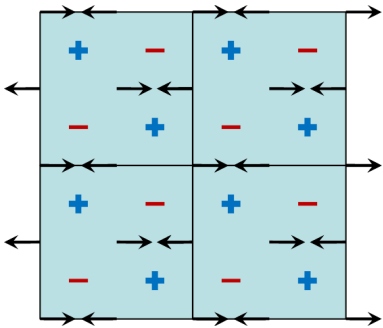
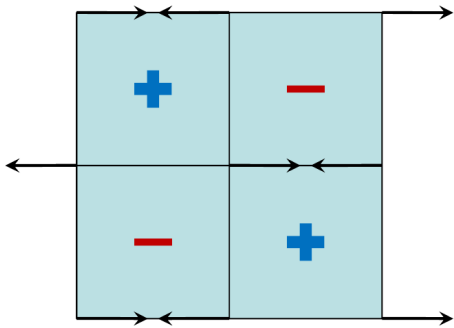
# Hourglass / Checkerboard Modes

We define an hourglass mode to be any continuous velocity mode that has non-zero divergence, but zero discrete divergence<sup>[1]</sup>

$$\vec{\nabla} \cdot \vec{v} \neq 0$$



$$\mathbf{D}_z \mathbf{v}_z = 0$$



[1] Idea proposed by V. Dobrev and T. Kolev

# The Noh Implosion Problem

## Tests:

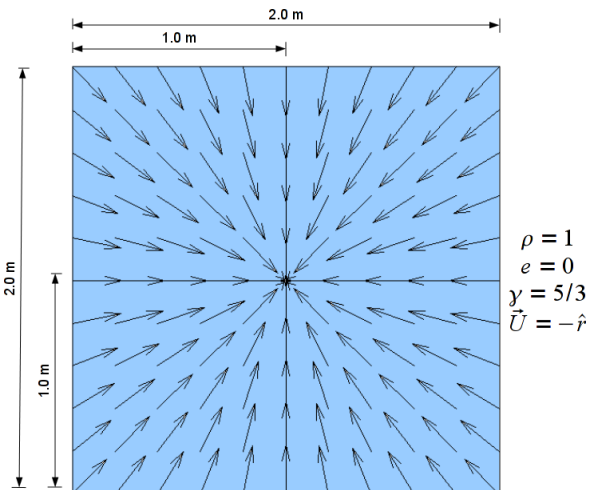
- Compression problems
- Symmetry preservation
- Artificial viscosity
- Shock speed
- Strong shocks

## Ideally:

- Postshock density = 16
- Shock travels at speed of  $1/3$
- Sharp shock front

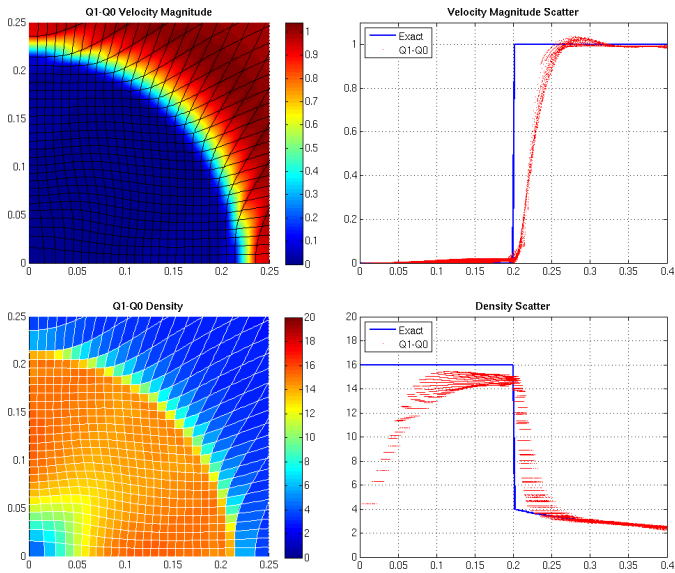
## Known Issues:

- “Wall heating” numerically “heats” the zone at the origin



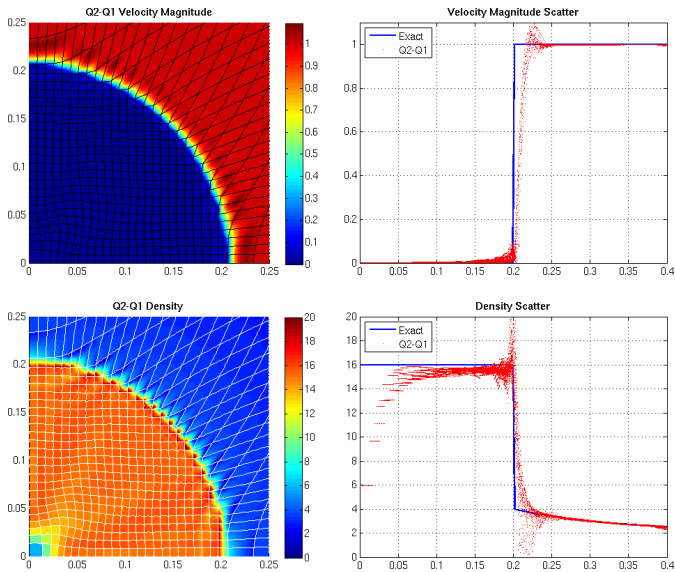
# Noh Implosion Problem, 30 by 30 Mesh: Q1-Q0

- Shock is not well resolved on this coarse mesh
- No overshoots or undershoots are observed



# Noh Implosion Problem, 30 by 30 Mesh: Q2-Q1d

- 36 plot points per zone
- Shock is more sharply resolved
- Wall heating is diminished
- Post shock density is closer to correct value
- Strong undershoots and overshoots in the density are observed in the single layer of zones at shock front



# The Saltzman Piston Problem

## Tests:

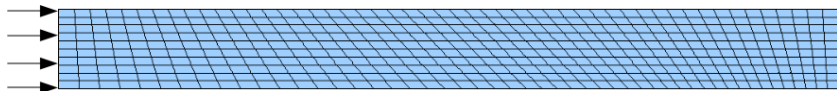
- Artificial viscosity
- Shocks that are not aligned with the mesh
- Shock-mesh interaction
- Mesh tangling

## Ideally:

- Post-shock density = 20
- Pre-shock density = 10
- Shock line is vertical
- Horizontal mesh lines stay that way

## Known Issues:

- “Wall heating” at both ends



$$V_L = 1.0$$

$$\rho_0 = 1.0$$

$$p_0 = 0$$

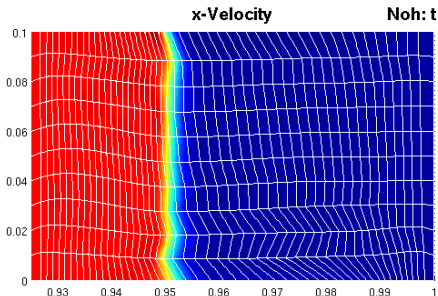
$$\gamma = 5/3$$

$$\vec{U}_0 = \vec{0}$$

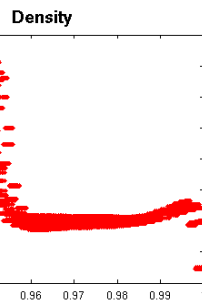
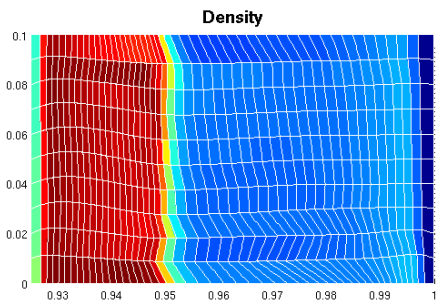
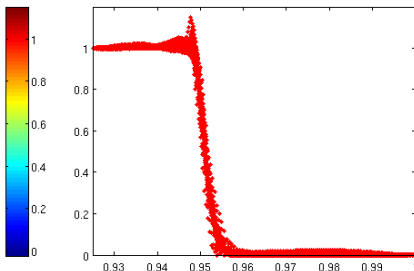
$$V_R = 0$$

Simulation will run till  $t = 0.925$

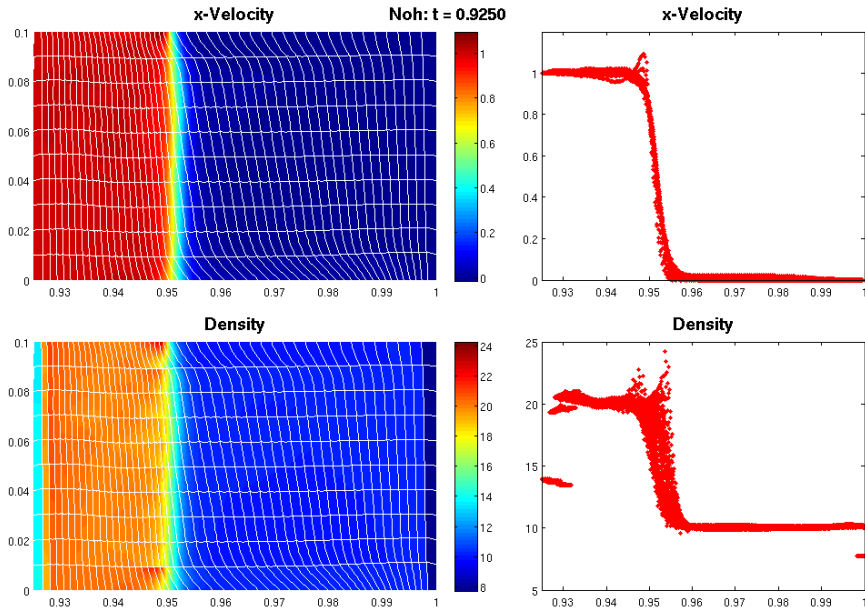
# Saltzman Piston Problem, 50 by 10 Mesh: Q1-Q0



Noh: t = 0.9250



# Saltzman Piston Problem, 50 by 10 Mesh: Q2-Q1d



# The Sedov Explosion Problem

## Tests:

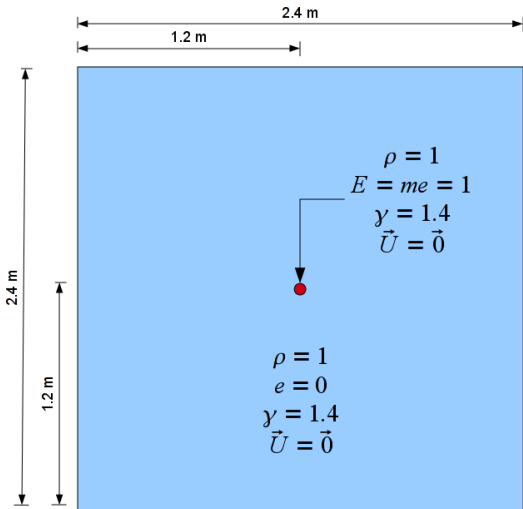
- Expansion problems
- Curved phenomena
- Correct maximum density

## Ideally:

- Maximum density = 6
- Circular shock
- Curved zones close to analytical mesh
- Sharp shock front
- No velocity oscillations

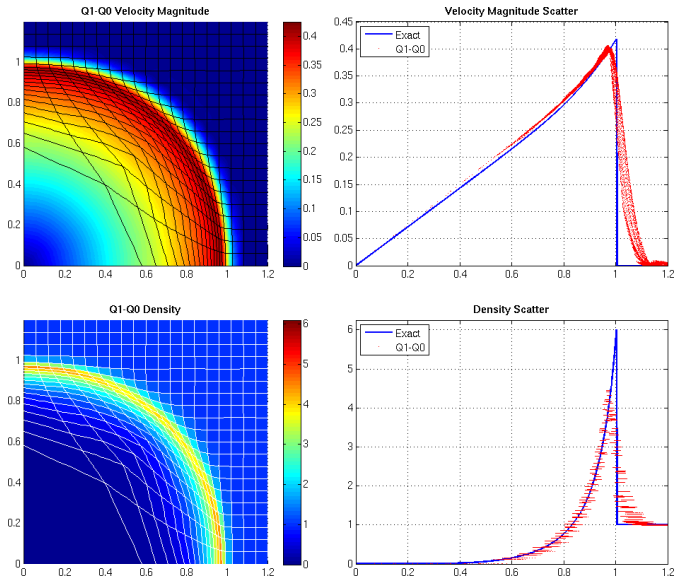
## Known Issues:

- Hourglass modes render  $Q_1 - Q_0$  solution impossible without filter



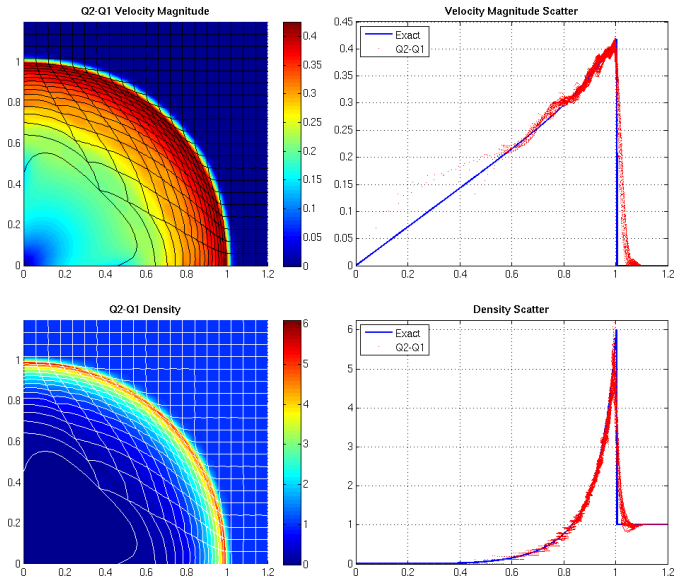
# Sedov Explosion Problem, 20 by 20 Mesh: Q1-Q0

- Standard HG filter required
- Shock is not well resolved on this coarse mesh
- Zone at origin has straight edges



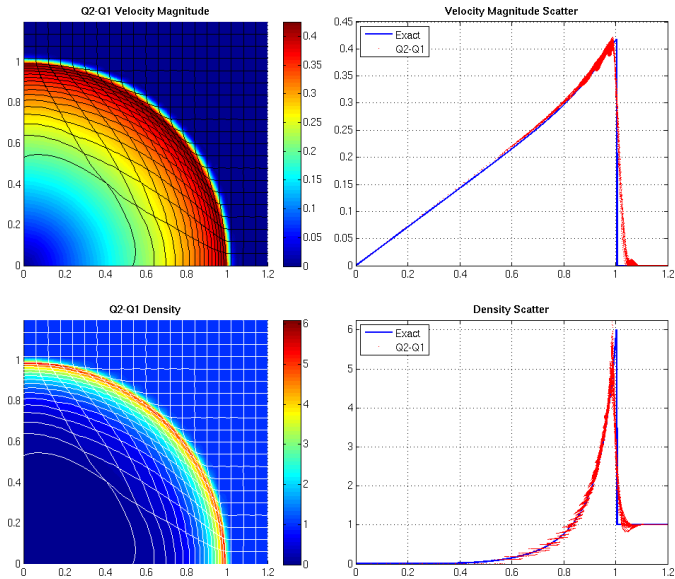
# Sedov Explosion Problem, 20 by 20 Mesh: Q2-Q1d

- No HG filter used
- Curved elements
- 81 plot points used per cell
- Shock front is much sharper on the same mesh
- Zone at origin has incorrect deformation
- Velocity oscillations are observed in post shock region

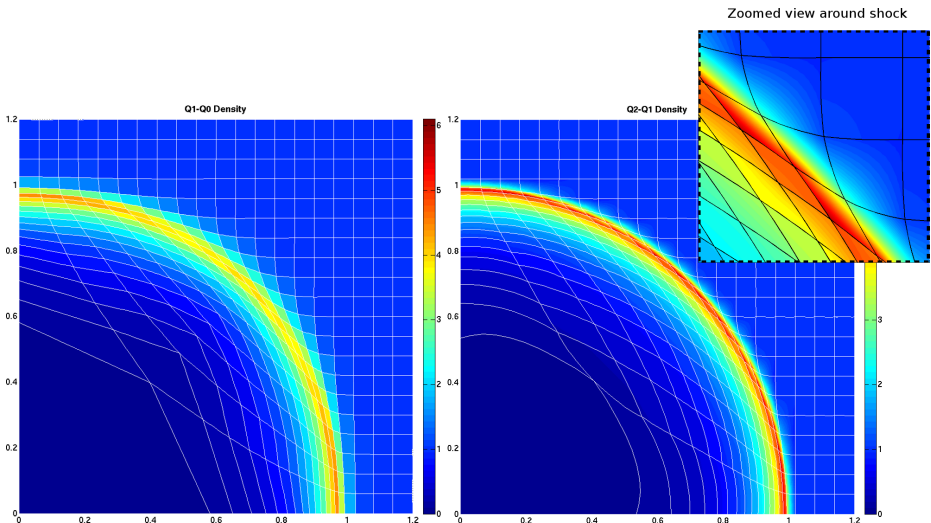


# Sedov Explosion Problem, 20 by 20 Mesh: Q2-Q1d

- No HG filter used
- 81 plot points used per cell
- Allowing 25% of the linear-q term in expansion has a significant benefit
- Velocity oscillations in post shock region are eliminated
- Curved deformation of zones closely resembles exact deformation
- We have not taken full benefit of the high order information in each cell to compute the viscosity coefficient, this is an area we plan to investigate much further

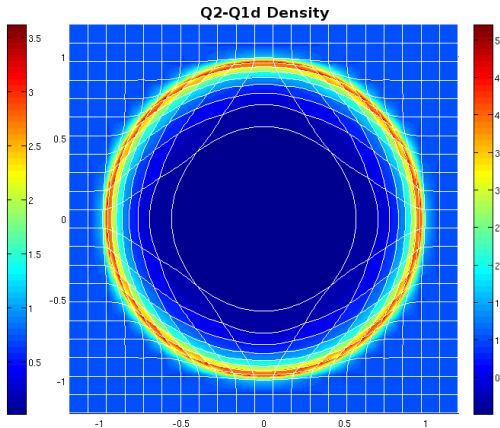
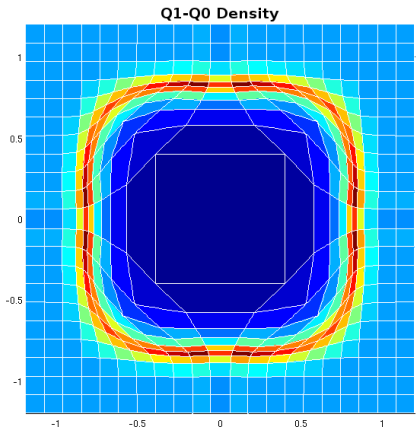


# Sedov Explosion Problem, 20 by 20 Mesh Comparison



# Sedov Explosion Problem, Full Mesh Comparison

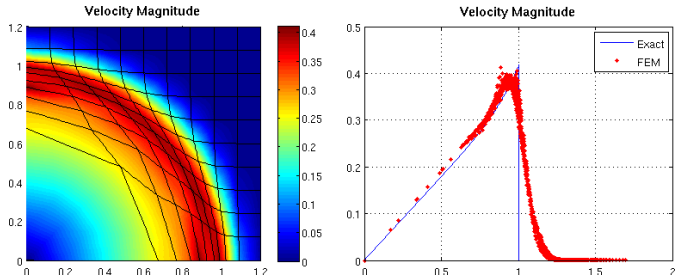
- High order methods naturally represent curved zones
- Low order methods lack the flexibility to model curved phenomena
  - Simulation crashes at  $t = 0.868$



# Other Elements Considered: Q1-Q1d

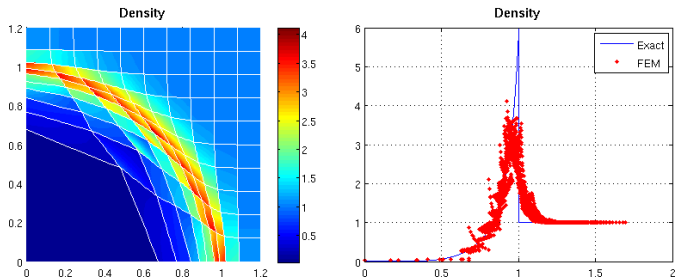
## Noh:

- More stable than Q1-Q0
- Less accurate than Q2-Q1d



## Saltzman:

- Straighter shock than Q1-Q0
- Wavy horizontal mesh lines



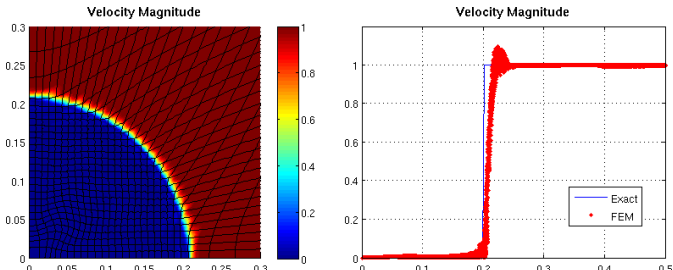
## Sedov:

- More circular shock than Q1-Q0
- Better maximum density than Q1-Q0
- Does not require hourglass filter
- Straight-edged zones

## Other Elements Considered: Q2-Q2d

### Noh:

- Limits density undershoots
- Exacerbates density overshoots

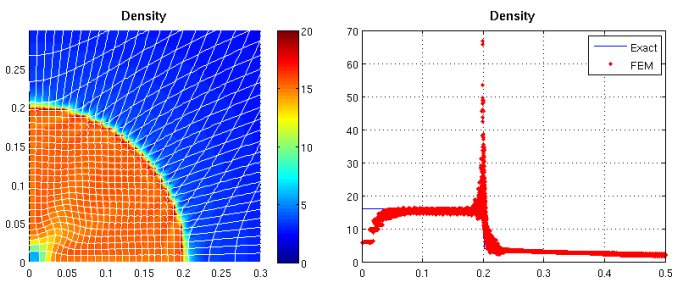


### Saltzman:

- Runs without hourglass filter
- Inferior to Q2-Q1d

### Sedov:

- Spurious oscillations
- Negatively curved zones
- Requires hourglass filter
- More accurate than low order methods



# Computational Efficiency

- Low order methods require  $2^{nD}$  elements for comparable accuracy
- Many calculations are done zone-by-zone
- Putting more of the computational burden on each zone increases computational efficiency

## High order element speedup

**Sedov Explosion Problem**

Method	36 Degrees of Freedom		121 Degrees of Freedom		441 Degrees of Freedom	
	Run Time	Speedup	Run Time	Speedup	Run Time	Speedup
$Q_1 - Q_0$	28.154	1.0	156.021	1.0	1265.232	1.0
$Q_1 - Q_{1d}$	29.565	0.95	165.185	0.94	1291.628	0.98
$Q_2 - Q_{1d}$	16.328	1.72	73.375	2.13	623.658	2.03
$Q_2 - Q_{2d}$	17.017	1.65	77.632	2.01	663.122	1.91

**Noh Implosion Problem**

Method	36 Degrees of Freedom		121 Degrees of Freedom		441 Degrees of Freedom	
	Run Time	Speedup	Run Time	Speedup	Run Time	Speedup
$Q_1 - Q_0$	101.192	1.0	383.356	1.0	1543.319	1.0
$Q_1 - Q_{1d}$	103.048	0.98	396.967	0.97	1590.766	0.97
$Q_2 - Q_{1d}$	53.042	1.91	191.063	2.01	775.230	1.99
$Q_2 - Q_{2d}$	53.605	1.89	194.381	1.97	792.363	1.95

# Conclusions

We have developed a general FEM framework for Lagrangian CFD

- Kinematic and thermodynamic space can be chosen independently
- For triangles:
  - Linear, quadratic, cubic, etc. kinematic space
  - Constant, linear, quadratic, etc. thermodynamic space
- For quads:
  - Bi-linear, bi-quadratic, bi-cubic, etc. kinematic space
  - Constant, bi-linear, bi-quadratic, etc. thermodynamic space
- This allows us to experiment with many different finite element pairs

We have also demonstrated that high order Lagrangian methods have significant promise

- Permits curved elements
- Increased accuracy
- Sharper shocks
- Density/pressure gradients in a single cell
- Second derivatives of velocity in a single cell
- Potential improvements for sub-zonal physics / multi-material ALE
- Post shock ringing is still an issue and we plan to address this by improving the artificial viscosity coefficient (e.g. the Hyper Viscosity technique of Cook and Cabot)
- More computationally efficient

# Questions?

